ITC 3/53
Information Technology and Control
Vol. 53 / No. 3/ 2024
pp. 932-942
DOI 10.5755/j01.itc.53.3.35708

A Lung Image Deep Learning Detection Model Based on Cross Residual Attention and Multi-feature Fusion

Received 2023/11/23 | Accepted after revision 2024/03/05

HOW TO CITE: Gou, H., Zhao, F., Tang, M., Zhang, G., Zhao, M. (2024). A Lung Image Deep Learning Detection Model Based on Cross Residual Attention and Multi-feature Fusion. *Information Technology and Control*, 53(3), 932-942. https://doi.org/10.5755/j01.itc.53.3.35708

A Lung Image Deep Learning Detection Model Based on Cross Residual Attention and Multi-feature Fusion

Haosong Gou
China Mobile Group Sichuan Co., Ltd., Chengdu 610041, Sichuan Province, China;
e-mail: gouhaosong@sc.chinamobile.com

Fanjie Zhao, Mingwei Tang
School of Computer and Software Engineering, Xihua University, Chengdu 610039, Sichuan Province, China;
e-mail: tang4415@126.com

Gaoyi Zhang
China Mobile Group Sichuan Co., Ltd., Chengdu 610041, Sichuan Province, China;
e-mail: gouhaosong@sc.chinamobile.com

Mingfeng Zhao
China Mobile Group Design Institute Co., Ltd. Sichuan Branch, Chengdu 610045, Sichuan Province, China;
e-mail: zhaomingfeng@cmdi.chinamobile.com

Corresponding authors: gouhaosong@sc.chinamobile.com, tang4415@126.com, zhaomingfeng@cmdi.chinamobile.com

Deep learning has become one of the hottest topics in medical image processing due to the development of deep learning technology. Currently, medical image research and applications suffer from two problems: a lack of data sets and an imbalance of classification categories. To solve these problems, we propose a method of residual attention and multi-feature fusion for lung image detection. Firstly, to integrate micro- and macro-feature extraction for medical image processing, two independent residual fusion strategies are designed, namely the Cross Residual Feature Extraction module (CRFE) and the Residual Attention Module (RAM). Secondly, a three-channel mechanism is designed for the Image Compensation Model (IFM). Using three channels and two residual fusion strategies, a multi-composite fusion architecture is produced to improve classifier performance. Finally, experimental results demonstrate that the proposed model performs better than the latest algorithms when compared with other medical image compensation methods.

KEYWORDS: Cross residual feature extraction, Residual attention, Cross-entropy fusion, Residual fusion strategy.

1. Introduction

AI-based image analysis and processing has become one of the hottest areas in research with the development of machine learning technology [25]. Deep learning technology has broad prospects in medical image processing [21]. Using fewer labels, Lu et al. proposed boundary-enhanced semi-supervised retinal layer segmentation [9]. Based on previous neural network models, Tang et al. proposed the residual graph attention network model [18]. Sethy et al. [16] proposed a hybrid network for the categorization of lung histopathology images. Nazir at al. proposed a machine learning-based lung cancer detection using multiview image registration and fusion [11].

Using multi-stream multi-scale convolutional networks, Ciompi et al. present a deep learning system that automatically classifies all nodule types relevant for nodule diagnosis [1]. K. Sherin et al. proposed an efficient deep learning approach for optimising lung cancer screening through advanced techniques [6]. In order to establish a lung cancer recognition model, an ANN algorithm model was selected [5]. In order to overcome these challenges, Poonkodi et al. proposed a novel approach for segmenting lung tumors [13]. Yan proposed an optimal lung cancer detection method based on CNN optimized and improved Snake optimization [27]. It is difficult to adjust these hyper-parameters physically, which determines the efficacy of this system. Therefore, an optimized convolution neural network is suggested in this study and is then employed to identify lung cancer types [12].

To address the above issue, this paper proposes a lung cancer research model based on image compensation and residual attention mechanisms. This primary contributions of this work can be summarized as follows: (1). To integrate micro- and macro-feature extraction for medical image processing, we propose two different residual fusion strategies, namely the Cross Residual Feature Extraction module (CRFE) and the Residual Attention Module (RAM). (2). In order to fully utilize the features in different branches, the cross-residual feature extraction module exchanges information directly between them. (3). A three-channel fusion mechanism is used in the Image Compensation Model (IFM).

2. Related Work

Nazir at al. proposed a machine learning-based lung cancer detection using multiview image registration and fusion in 2023 [11]. Small medical image training sample data can be solved with this network model. Xia et al. [25] were able to obtain more parameters from MRI images. As a result of its experimental results, the area under the ROC curve (AUC) was 0.968, and the accuracy was 94.7% [17].

Using MRI texture features, Zhao et al. [31] developed CAD glioma grade prediction accuracy as high as 86.8%, with an AUC of 0.89. Using artificial intelligence, different brain tumors can be differentiated minimally or noninvasively in the future [20]. Based on multi-parameter MRI images, Litjens et al. developed a support vector machine (SVM) classifier prediction model [19]. Using multi-parametric MRI and a random forest classifier, Suh et al. distinguished primary central nervous system lymphoma from atypical glioblastoma [2]. According to Raj et al. [14], LSTM and CNNs are combined to form a neural network model [23]. By using over-complete techniques, information loss can be reduced, and structural information in the data can be mined [10]. Zhang et al. proposed a joint sparse model with coupled dictionary for medical image fusion [29].

As a result, the data can be structured more easily. Data underlying any underlying statistical distribution can be better approximated with an overcomplete basis [17]. Similarly, it is widely used for resolving mixed signals that contain information and noise [2]. It is shown that the denoising idea of autoencoders proposed by Valanarasu et al. improves the feature detection capabilities of fully complete networks, as well as its performance is superior to the standard bottleneck structure [19]. The field of neuroscience, which addresses the problem of maintaining stable sensory perception in the absence of sustained activity, is also supported by overcomplete characterization in neuroscience [7].

3. Method

This paper proposes two different residual fusion strategies, namely the Cross Residual Feature Extraction module (CRFE) and the Residual Attention

Module (RAM). A three-channel mechanism is used in the Image Compensation Model (IFM).

3.1. Definition of the Problem

Initially, this paper designs a classifier to distinguish malignant pulmonary nodules from benign nodules [30]. Sample space X and label set $Y \in \{0, 1\}$ represent the sample space and label set, respectively. Imagine that a classifier is constructed using the representation F, and that the classifier is based on a nonlinear mapping $F(x) \to Y$. There are T_+ and T_- samples being examined, respectively, and the total number of samples is T. Malignant samples are indicated by X^+, benign samples by X^-, and the total number of samples is T. Based on Equation (1), the accuracy (ACC) of mapping F onto the sample space X can be expressed as follows:

$$ACC(F,X) = \frac{\sum_{i=1}^{T_+} \mathrm{II}[F(x_i^+) > 0.5] + \sum_{j=1}^{T_-} \mathrm{II}[F(x_j^-) \le 0.5]}{T_+ + T_-} . \quad (1)$$

$\mathrm{II}[\cdot]$ is the indicator function. If the parameter is true, it returns 1; if false, it returns 0. According to AUC, F maps onto X as follows:

$$ACC(F,X) = \frac{\sum_{i=1}^{T_+} \mathrm{II}[F(x_i^+) > 0.5] + \sum_{j=1}^{T_-} \mathrm{II}[F(x_j^-) \le 0.5]}{T_+ + T_-} . \quad (2)$$

The ACC measures the difference between labeled model outputs. As a result, AUC mainly measures the difference between positive and negative rankings. AUC and ACC are being improved in this article. It is possible to eliminate the effects of these factors on the performance index during training, however, when the data set is small and the classes are unbalanced.

3.2. Detailed Description of the Model

3.2.1. Cross Residual Feature Extraction Module (CRFE)

Convolutional neural networks (CNNs) are often improved through methods of increasing their depth. When network layers increase, gradients may disappear or explode during backpropagation. Therefore, when propagating through the network, after multiplying the error value by the weight, the weight value may gradually decrease, causing the gradient to approach zero. When this phenomenon occurs, the neural network's learning will first show an upward trend during the training process, but then stabilize and reach saturation. If the weights are further optimized, a neural network may not be able to achieve higher accuracy.

To further improve the performance and accuracy of convolutional neural networks, network designers must adopt other strategies or techniques to solve the vanishing or exploding gradient problem. In addition to batch normalization, residual connections may be introduced, or the network structure may be adjusted using these strategies. As shown in Figure 1, the residual block framework consists of the following blocks:

$$H(x) = F(x) + x \to F(x) = H(x) - x . \quad (3)$$

The residual module input is x, and the residual module output is $F(x)+x$. The residual is $F(x)$ as long as $F(x)=0$ is an identity map $H(x)$.It is actually implemented using a feedforward neural network with shortcut connections, which are just simple identity mappings. Increasing network depth will improve network performance. The residual neural network (ResBlock) can avoid the above situation, but it will add additional parameters. The computational complexity of the network is not increased by residual learning.

Figure 1
Cross residual feature extraction module

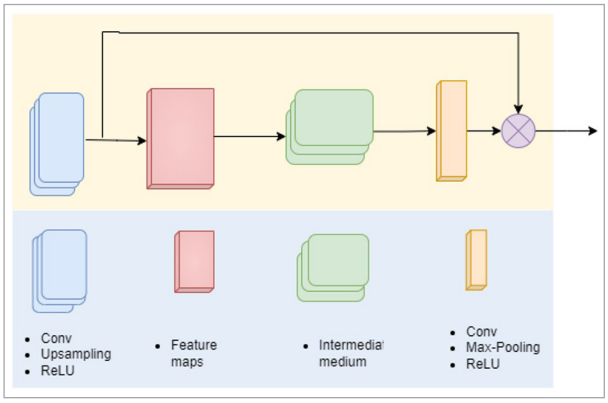

Based on the traditional residual network model structure, this paper proposes a cross residual feature extraction module (CRFE) based on actual and current medical image processing needs. In order to fully utilize the features in different branches, the cross-residual feature extraction module exchanges information directly between them. Through the convolution layer, upsampling layer, and ReLU acti-

vation function, the intermediate medium block (intermediate medium) is obtained in the cross-residual feature extraction module. On the intermediate medium block, convolution, maximum pooling, and ReLU function activation are performed, and finally the obtained feature map is merged with the input map.

3.2.2. Residual Fusion Strategy (RFS)

As part of the training phase, we propose a residual fusion strategy that uses features collected from three channels to fuse the images. The macro channel ZL-Net (OA), micro channel ZL-Net (DT) and general channels are used to process original images with different pixel ratios. Different scales and perspectives are extracted from these three channels. A feature cluster is formed by integrating information from the three channels using the cross-residual feature block. With a residual attention module, the model is further enhanced to capture the importance of features in different branches during training and learning, and to weight the features of different branches in real-life situations. For feature extraction and information transfer, the processed image clusters are input into the residual block of the four-layer structure in the experimental stage. By using the residual block, the vanishing gradient problem can be effectively solved and the network's performance can be improved. To complete the processing, the residual block output is fused with the original image. As shown in Figure 2, the residual fusion strategy is illustrated. As a result, the construct is trained using these cropped multi-scale patches. In Equation (4), the final result is calculated by combining the three trained models.

$$F_{Ensemble} = w_0 F_{32}(X') + w_1 F_{48}(X') + w_2 F_{64}(X'). \quad (4)$$

In this case, $F*$ represents the sub-model trained using multi-size cropped CT images. According to grid search, the integration weights w_0, w_1, w_2 are determined.

3.2.3. Cross-entropy Loss (CEL)

In order to solve the imbalance problem, data-level classification is commonly used, which usually involves oversampling and undersampling. In contrast, this method does not increase the diversity of training samples and can easily lead to overfitting. An alternative approach when the diversity of the data set remains the same is to modify the performance index. In general, the CEL function is defined as follows:

$$F_{Ensemble} = w_0 F_{32}(X') + w_1 F_{48}(X') + w_2 F_{64}(X'). \quad (5)$$

Wang et al. [24] propose the AUC approximation function to implement an indicator that is insensitive to imbalanced categories. Because it can be classified as a combinatorial optimization problem, directly using the AUC defined in the equation part often leads to NP-hard problems.

As an explicit optimization problem, AUC optimization is converted or approximated in practical applications. Gao et al. [3] propose a new approximation method, where $F(x_i^+) - F(x_i^-) \le 0$ and I are computational constraints. The following equation can then be shown as in Equation (6).

$$\begin{aligned} AUC(F,X) &= \sum_{i=1}^{T_+}\sum_{j=1}^{T_-}\frac{\mathrm{II}[F(x_i^+) > F(x_i^-)] + \frac{1}{2}\mathrm{II}[F(x_i^+) = F(x_i^-)]}{T_+T_-} \\ &\approx \sum_{i=1}^{T_+}\sum_{j=1}^{T_-}\frac{\mathrm{II}[F(x_i^+) > F(x_i^-)]}{T_+T_-} \\ &= 1 - \sum_{i=1}^{T_+}\sum_{j=1}^{T_-}\frac{\mathrm{II}[F(x_i^+) \le F(x_i^-)]}{T_+T_-} \end{aligned} \quad (6)$$

Figure 2
Residual fusion strategy

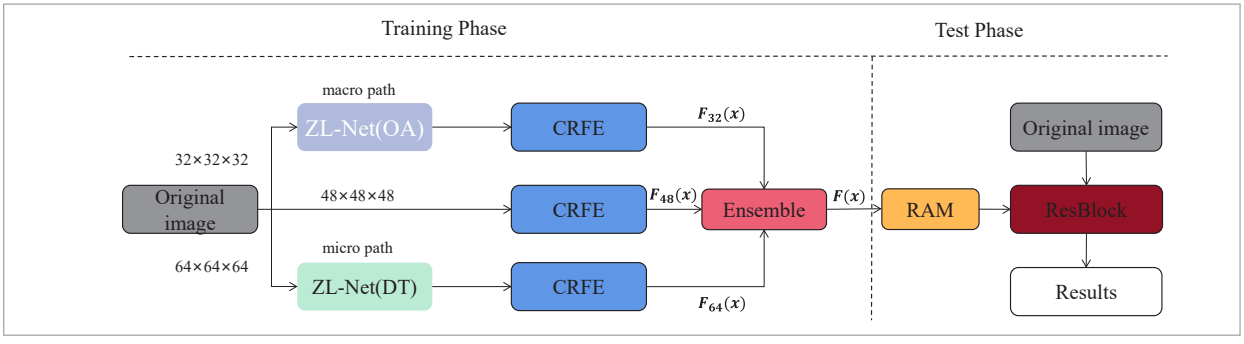

Figure 3
Image compensation model diagram

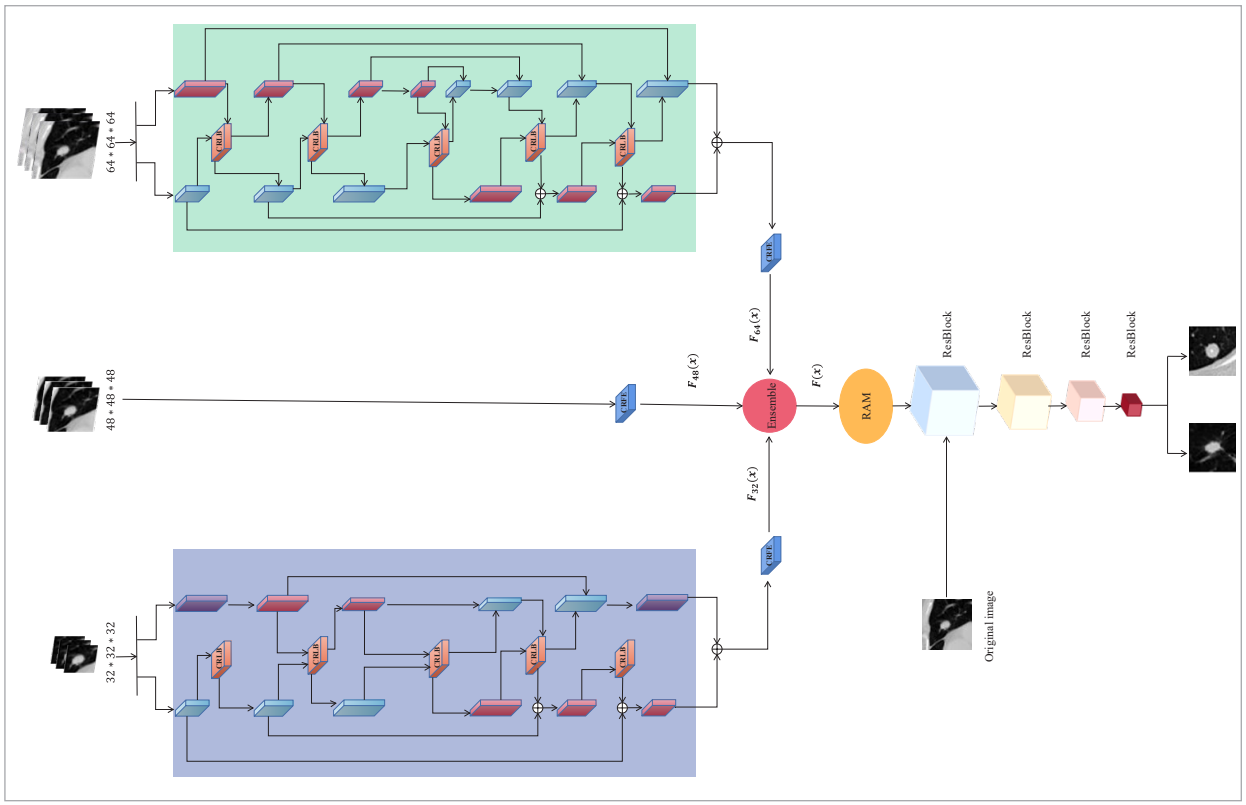

Therefore, the design formula of this article is as shown in (6), which represents the target item that needs to be optimized as shown as in Equation (7).

$$l(F,X^+,X^-)=\sum_{i=1}^{T_+}\sum_{j=1}^{T_-}\frac{\mathrm{II}F(x_i^+)-F(x_i^-)\le 0}{T_+T_-}. \tag{7}$$

Therefore, the design formula of this article is as shown in (6), which represents the target item that needs to be optimized.

$$l_{hinge}(F,X^+,X^-)=\max(0,1-(F(X^+)-F(X^-))). \tag{8}$$

Moreover, F in this study is a nonlinear map whose output is limited to the range $(0,1)$, $F(X)\in(0,1)$

$$\begin{aligned}&-(F(X^+)-F(X^-))\in(-1,1)\\&1-(F(X^+)-F(X^-))\in(0,2)\end{aligned} \tag{9}$$

From Equation (9), $1-(F(X^+)-F(X^-))$ is always greater than zero. Accordingly, Equation (10) is equivalent to the next equation in this study.

$$\begin{aligned}l_{hinge}(F,X^+,X^-)&=1-(F(X^+)-F(X^-),\\&=\sum_{i=1}^{T_+}\sum_{j=1}^{T_-}\frac{1-(F(x_i^+)-F(x_i^-))}{T_+T_-}\end{aligned} \tag{10}$$

In Equation (8), there is an approximation when F is a linear classifier, i.e. $F(x)=W^TX$. According to AUC [4], which is based on the squared loss as follows, this method is inconsistent with AUC:

$$l_{square}(F,X^+,X^-)=\sum_{i=1}^{T_+}\sum_{j=1}^{T_-}\frac{(1-(F(x_i^+)-F(x_i^-)))^2}{2T_+T_-}. \tag{11}$$

There are significant advantages to this indicator function, since it proves that when F is a linear mapping, the squared loss is consistent with the AUC [3]. Additionally, this approach is independent of the number of training examples. According to Equations (10)-(11), the former is a first-order penalty term, while the latter is a second-order penalty term. The following surrogate lossy power function is developed for nonlinear mappings F:

$$l_{\lambda}(F,X^{+},X^{-})=\sum_{i=1}^{T_{+}}\sum_{j=1}^{T_{-}}\frac{(1-(F(x_i^{+})-F(x_i^{-})))^{\lambda}}{\lambda T_{+}T_{-}}, \quad (12)$$

where $\lambda \in R^{+}$ .With a small number of samples, this paper is able to improve the classifier's performance. Furthermore, this paper introduces a new loss function, based mainly on the CEL term and the AUC penalty loss term. A proposed loss function is shown below Equation (13).

$$L_{AUG_{CEL}}=L_{CEL}+\alpha\cdot l_{\lambda}(F,X^{+},X^{-}), \quad (13)$$

where, $\alpha \in R^{+}$ is the coefficient AUC in the loss term of the AUC. For 32, 48, and 64 sizes, α adopts the corresponding values of 0.5, 0.75, and 1 [26].

3.2.5. Image Compensation Module (IFM)

For more effective information extraction and fitting, the image compensation module employs a tri-channel mechanism with cross-residual feature blocks (CRFE). A reconstructed feature cluster is then constructed using these feature information. A residual attention module (RAM) is also introduced to enhance the model's performance by compensating for information features extracted from the original image. In residual fusion, key information in medical images is captured using residual networks based on this framework.

To integrate multi-pixel image features, the model uses a novel loss function to take into account the contribution of each pixel during the optimization process. To obtain a more accurate classification of benign and malignant tumors, the model uses an information exchange module to interact with image features. As a result of this innovative method, clinicians can expect a higher level of accuracy in tumor diagnosis.

4. Results of Experiments and Analyses

4.1. Dataset

Using LIDC-IDRI, physicians annotate pulmonary nodules' malignancy based on their morphology. The malignant pulmonary nodules are clearly irregular and have lobular, needle-like, cavity-like, and other shapes. The edges of benign pulmonary nodules are sharper and more regular. Due to their lack of calcification, some malignant lung nodules are not brighter than benign lung nodules. The clinical definition of low density is that it is too low to be malignant. There is a higher likelihood that larger lung nodules are malignant based on this figure.

Table 1
Dataset sheet

LIDC-DRI	Benign	Uncertain		Malignant	
MML	1	2	3	4	5
numbers	325	831	957	436	120

There are 1018 clinical chest CT scans of pulmonary nodules in the LIDC-IDRI database, which is available from the Archives of Cancer Imaging [22]. The CT image is accompanied by an XML file detailing the location of the nodule. It is generally accepted that some suspicious lesions merge into the same pulmonary nodule, if the center of the lesions is located in a different area. There is a main focus on nodule diameters over 3 mm in this article. The total number of lung nodules obtained by this paper is 2669.

1 Construction and preprocessing of data sets

For training and testing, all lung nodules are cropped from the original CT images. Using NumPy, a 64-pixel 3D path was extracted from the CT image around the lung nodule's center for preprocessing. Each pixel in the original cropped patch contains its CT value (V_{ct}). To map CT values to V levels in the range [0,1], the following Equation (14) is used.

$$V=\begin{cases}0, & V_{ct}\le -1000\\ \dfrac{V_{ct}+1000}{1400}, & -1000\le V_{ct}\le 400\\ 1, & V_{ct}\ge 400\end{cases} \quad (14)$$

As part of the training process, this paper crops plaques of different sizes from images of the lesion centers that have been preprocessed. Additionally, samples are flipped and translated to increase their diversity. Firstly, the input is passed through two convolutional layers and then through a maximum pooling layer (MP). Through a global average pooling layer, the last block is converted into feature vectors. Secondly, there is a layer that is fully connected and a layer that is output. There are three subnetworks in

Figure 4
The malignant samples cropped from lung CT images

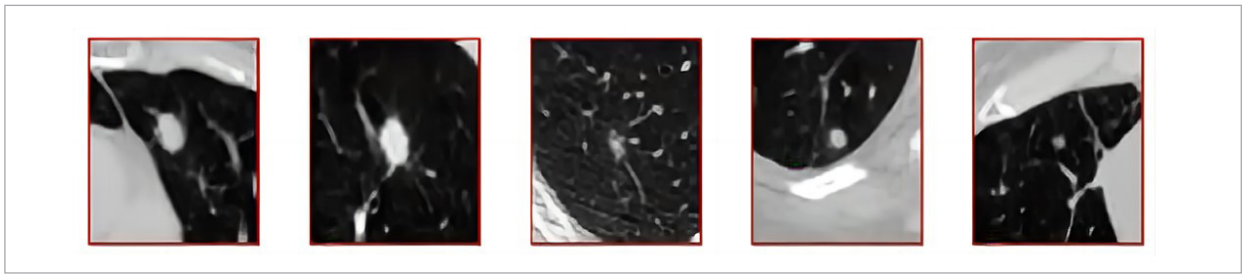

Figure 5
The Benign samples cropped from lung CT images

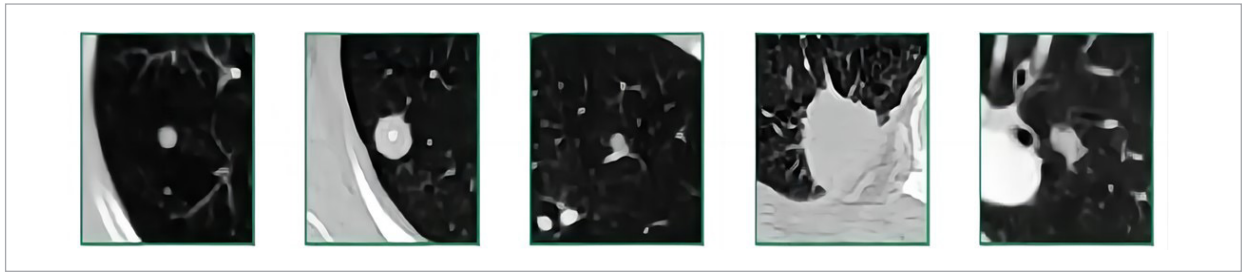

this article, whose structures are identical except for the input size. To obtain the final integration result, these three subnets are combined. As a result of the limited data sets, this study employs optical networks in which each subnet contains ten layers. To improve the performance of this model under imbalanced categories, we introduce a loss function that incorporates cross-entropy and AUC.

2 Enhancement of the data

An ensemble of lightweight models is used in this article as an alternative solution. It is easier to solve the overfitting problem with lightweight models because they have fewer parameters than large models. Multi-lightweight models are used in this paper to evaluate the task in an integrated manner. In this case, 2D convolutional neural networks are usually used as the backbone network. The decomposition process, however, may result in a loss of heterogeneity in lung nodules. A three-dimensional convolutional neural network is used as the backbone network in this paper.

4.2. Index of Experimental Evaluation

There are four commonly used evaluation indicators in the model: Accuracy ($Acc = \frac{TP + TN}{TP + FP + TN + FN}$), Precision ($P = \frac{TP}{TP + FP}$), Recall ($R = \frac{TP}{TP + FN}$) and F1 Score ($F1 = \frac{2 * P * R}{P + R}$). These four indicators are explained in detail below, along with their definitions and formulas.

4.3. Environment Settings for Experiments

The deep learning model in this article was developed using the Python programming language and Pytorch deep learning framework under a Linux environment. As shown in Table 2, detailed parameters of software and hardware are configured. A RTX 3090 (24GB) and CUDA 11.4 were used in this article. In Python 3.7 and Pytorch-v1.10.0, the designed network model is used.

Table 2
Environment settings for experiments

hardware	CPU	Intel(R) Core(TM) i9-10900X
	GPU	NVIDIA RTX 3090 24G
	Memory	64GB
	Disk	512G M.2 SSD
software	System	Ubuntu 18.04.5 Server
	Python	3.7.6
	Pytorch	1.10.0

4.4. Parameter Settings

As shown in Table 3, the parameter settings of the experimental model are described in this article.

Table 3
Training parameters

Parameter	Value
ResBlock layers	4
Batch size	120
Dropout	0.5
Optimizer	Adam
Learning rate	1e-3
Hidden layer size	486
Epoch	30

4.5. Results of Experiments

An evaluation was performed by calculating the mean and standard deviation of the Acc, sensitivity/recall, specificity, precision with a cutoff value of 0.5, F1 score and AUC. Model parameters are saved at the end of each epoch after 120 epochs of training.

In the beginning, learning rate *lr* is set to $1e-3$, and every 30 epochs it is changed to $lr = lr * 0.1$ again. In Table 4, the image compensation model proposed in this chapter successfully enables the model to extract a wider range of features from pulmonary nodules. MD stands for OL [9] MSCS-DeepLN [26], KiU stands for KiU-Net [19], DAS stands for DAS-Net [8], SD2023 [15], ZlOA stands for Zl-Net OA, ZlDT stands for Zl-Net DT, and IFM stands for the image fusion model. There are some suboptimal indicators, indicating that the model could be optimized, such as Precision and AUC. It is possible that the loss of features caused by the image reconstruction module may affect the quality of the image.

4.6. Ablation Experiments

A research on ablation is performed using the U-Net and the KiU-Net traditional over-complete architecture models. A residual fusion strategy is evaluated by analyzing the information loss of image information within a single data set. Furthermore, a spatially overcomplete network model and a traditional IMF image compensation model are compared. The LIDC-IDRI dataset was used in this experiment. Under a single data set, the information extraction degree and loss bias of each model are verified. In Table 4, it is shown that while U-Net captures a certain amount of image detail features, it cannot capture features like KiU-Net and IFM (the proposed image fusion model). The majority of these advanced features eventually lead to a severe loss of U-Net functionality. Based on an experimental comparison of the loss rate in the information extraction process with the KiU-Net model using an overcomplete architecture, it was found that KiU-Net still has a higher loss convergence than IFM. As shown in Figure 8, experimental results were obtained. As a result, residual fusion has been shown to be effective.

Table 3
Comparison experiment results

Model	Acc	Recall	Precision	AUC	F1 Score
OL	93.11±0.18	-	-	-	-
SD2023	93.40±0.16	-	-	-	-
MD	92.65±0.26	85.58±0.94	90.39±0.94	94.00±0.25	87.91±0.43
KiU	92.06±0.28	83.62±0.51	90.27 ± 1.28	93.88 ± 0.17	86.82 ± 0.33
DAS	92.17±0.23	84.55±0.37	90.78 ± 0.21	92.58 ± 0.24	86.98± 0.12
ZlOA	92.78± 0.17	84.68 ± 1.23	**91.95 ± 0.60**	93.78 ± 0.23	87.16 ± 0.41
ZlDT	92.12 ± 0.23	84.36 ± 1.64	89.80 ± 0.75	**94.35 ± 0.37**	87.98 ± 0.54
IFM	**93.65±0.26**	**87.58±0.94**	90.89±0.94	94.00±0.25	**88.91±0.43**

5. Conclusion

In this paper, we propose a medical image network model that enhances energy by merging medical image compensation with special effects information extraction. There are three advantage modules in the network model: a full feature extraction module, a feature fusion module, and an image reconstruction module. In the full feature extraction module, multi-scale and multi-dimensional feature extraction mechanisms are used. Multiple parallel medical images are extracted and merged using a residual fusion strategy. The fused features are then fed into the image reconstruction module. Multidimensional image extraction in the feature extraction module can better extract detailed information from medical images. There is room for future research to incorporate a broader range of models, datasets, and metrics.

Acknowledgement

This work is supported by the project of new technology research (R22109V6) funded by the postdoctoral programme of China Mobile Communications Group Sichuan Co., Ltd, the National Natural Science Foundation of China (No. 61902324), Funds Project of Chengdu Science and Technology Bureau (No. 2023-JB00-00020-GX).

Table 4

Ablation experiment results

Method	Dice	Jaccard
U-Net	0.8279	0.7502
KiU-Net	0.8943	0.8326
Zl-Net(OA)	0.9008	0.8456
Zl-Net(DT)	0.7159	0.8538
CEL	0.8890	0.8520
IFM	**0.9017**	**0.8698**

Figure 5

Residual fusion strategy and convergence comparison of KiU-Net and U-Net loss

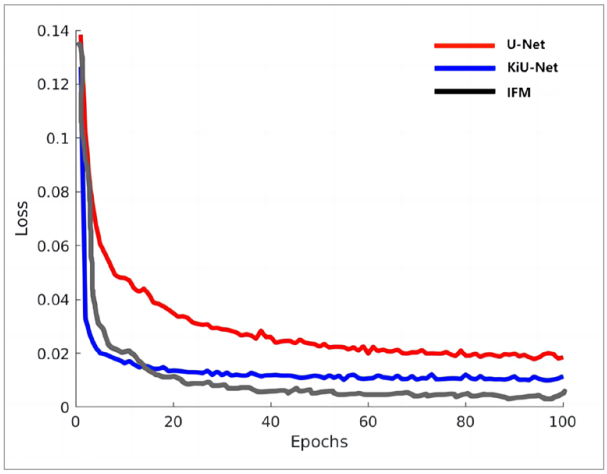

References

1. Badrinarayanan, V., Kendall, A., Cipolla, R. SegNet: A Deep Convolutional Encoder-Decoder Architecture for Image Segmentation. IEEE Transactions on Pattern Analysis and Machine Intelligence, 2017, 39(12), 2481-2495. https://doi.org/10.1109/TPAMI.2016.2644615
2. Esmaeili, M., Toosi, A., Roshanpoor, A., Changizi, V., Ghazisaeedi, M., Rahmim, A., Sabokrou, M. Generative Adversarial Networks for Anomaly Detection in Biomedical Imaging: A Study on Seven Medical Image Datasets. IEEE Access, 2023, 11, 17906-17921. https://doi.org/10.1109/ACCESS.2023.3244741
3. Gao, W., Wang, L., Jin, R., Zhu, S. H., Zhou, Z. H. One-Pass AUC Optimization. Artificial Intelligence, 2016, 236, 1-29. https://doi.org/10.1016/j.artint.2016.03.003
4. Gao, W., Zhou, Z. H. On the Consistency of AUC Optimization. CoRR, 2012, abs/1208.0645. http://arxiv.org/abs/1208.0645
5. He, B., Hu, W., Zhang, K. Image Segmentation Algorithm of Lung Cancer Based on Neural Network Model. Expert Systems, 2022, 39(3). https://doi.org/10.1111/exsy.12822
6. K. Sherin, M. E. Optimising Lung Cancer Screening Through Advanced Techniques for Image Analysis: An Efficient Deep Learning Approach. Proceedings of the Fourth International Conference on Smart Electronics and Communication (ICOSEC-2023). https://doi.org/10.1109/ICOSEC58147.2023.10275884
7. Lewicki, M. S., Sejnowski, T. J. Learning Overcomplete Representations. Neural Computation, 2000, 12(2), 337-365. https://doi.org/10.1162/089976600300015826
8. Luo, S., Zhang, J., Xiao, N., Xiao, N., Qiang, Y., Li, K. Q., Zhao, J. J., Meng, L., Song, P. DAS-Net: A Lung Nodule Segmentation Method Based on Adaptive Dual-Branch Attention and Shadow Mapping. Applied Intelligence,

2023, 52(13), 15617-15631. https://doi.org/10.1007/s10489-021-03038-2

9. Lu, Y., Shen, Y., Xing, X., Xing, X. H., Ye, C. W., Meng, M. Q. H. Boundary-Enhanced Semi-Supervised Retinal Layer Segmentation in Optical Coherence Tomography Images Using Fewer Labels. Comput. Medical Imaging Graph., 2023, 105, 102199. https://doi.org/10.1016/j.compmedimag.2023.102199
10. Nallasivan, G., Akshaya, V. S., Padmavathy, C. A Computational Model for Medical Image Retrieval Using Orthogonal Moment. Journal of Intelligent Fuzzy Systems, 2023, 44(2), 3261-3269. https://doi.org/10.3233/JIFS-221667
11. Nazir, I., Haq, I., Alqahtani, S. A. Machine Learning-Based Lung Cancer Detection Using Multiview Image Registration and Fusion. Journal of Sensors, Volume 2023, 2023. https://doi.org/10.1155/2023/6683438
12. Paikaray, D., Mehta, A.K., Khan, D. A. Optimized Convolutional Neural Network for the Classification of Lung Cancer. Journal of Supercomputing, 2023, 8. https://doi.org/10.1007/s11227-023-05550-3
13. Poonkodi, S., Kanchana, M. Lung Cancer Segmentation from CT Scan Images Using Modified Mayfly Optimization and Particle Swarm Optimization Algorithm. Multimedia Tools and Applications, 2023. https://doi.org/10.1007/s11042-023-15688-0
14. Raj, R. J. S., Shobana, S. J., Pustokhina, I. V., Pustokhina, I. V., Pustokhin, D. A., Gupta, D., Shankar, K. Optimal Feature Selection-Based Medical Image Classification Using Deep Learning Model in Internet of Medical Things. IEEE Access, 2020, 8, 58006-58017. https://doi.org/10.1109/ACCESS.2020.2981337
15. Santos, D. Tackling Lung Cancer: Advanced Image Analysis and Deep Learning for Early Detection. TechRxiv, June 18, 2023.
16. Sethy, P. K., Geetha, D. A., Padhan, B., Padhan, B., Behera, S. K., Sreedhar, S., Das, K. Lung Cancer Histopathological Image Classification Using Wavelets and AlexNet. Journal of X-Ray Science and Technology, 2023, 31(1), 211-221. https://doi.org/10.3233/XST-221301
17. Shen, T., Xu, H. Medical Image Segmentation Based on Transformer and HarDNet Structures. IEEE Access, 2023, 11, 16621-16630. https://doi.org/10.1109/ACCESS.2023.3244197
18. Tang, M. W., Tang, W., Gui, Q. C., Hu, J., Zhao, M. F. A Vulnerability Detection Algorithm Based on Residual Graph Attention Networks for Source Code Imbalance (RGAN). Expert Systems with Applications, 2024, 238(D), 162023. https://doi.org/10.1016/j.eswa.2023.122216
19. Valanarasu, J. M. J., Sindagi, V. A., Hacihaliloglu, I., Patel, V. M. Kiu-Net: Towards Accurate Segmentation of Biomedical Images Using Over-Complete Representations. International Conference on Medical Image Computing and Computer-Assisted Intervention, Springer, 2020, 363-373. https://doi.org/10.1007/978-3-030-59719-1_36
20. Vincent, P., Larochelle, H., Bengio, Y., Manzagol, P. A. Extracting and Composing Robust Features with Denoising Autoencoders. Proceedings of the 25th International Conference on Machine Learning, 2008, 1096-1103. https://doi.org/10.1145/1390156.1390294
21. Wang, H., Zhu, Y., Green, B. Axial-DeepLab: Stand-Alone Axial-Attention for Panoptic Segmentation. European Conference on Computer Vision, Springer, 2020, 108-126. https://doi.org/10.1007/978-3-030-58548-8_7
22. Wang, J., Zhang, B., Lin, L. A Software for the Lung Image Database Consortium and Image Database Resource Initiative. ICBBS 2019: 8th International Conference on Bioinformatics and Biomedical Science, Beijing, China, October, 2019, 59-63. https://doi.org/10.1145/3369166.3369192
23. Wang, P. C., Tao, L. P., Tang, M. W., Zhao, M. F., Wang, L. X., Xu, Y. S., Tian, J. X., Meng, K. Z. A Novel Adaptive Marker Segmentation Graph Convolutional Network for Aspect-Level Sentiment Analysis. Knowledge-Based Systems, 2023, 270, 110559. https://doi.org/10.1016/j.knosys.2023.110559
24. Wang, X., Han, S., Chen, Y., Gao, D. S., Vasconcelos, N. Volumetric Attention for 3D Medical Image Segmentation and Detection. International Conference on Medical Image Computing and Computer-Assisted Intervention, Springer, 2019, 175-184. https://doi.org/10.1007/978-3-030-32226-7_20
25. Xiong, J. Q., Tang, M. W., Zong, L. S., Li, L. X., Hu, J., Bian, D., Lv, S. X. INA-Net: An Integrated Noise-Adaptive Attention Neural Network for Enhanced Medical Image Segmentation. Expert Systems with Applications, 2024, 1-24. https://doi.org/10.1016/j.eswa.2024.125078
26. Xu, X., Wang, C., Guo, J., Gan, Y. C., Wang, J. Y., Bai, H. L., Zhang, L., Li, M. M., Yi, Z. MSCS-DeepLN: Evaluating Lung Nodule Malignancy Using Multi-Scale Cost-Sensitive Neural Networks. Medical Image Analysis, 2020, 65, 101772. https://doi.org/10.1016/j.media.2020.101772
27. Yan, C. H., Razmjooy, N. Optimal Lung Cancer Detection Method Based on CNN Optimized and Improved Snake Optimization Algorithm. Biomedical Signal Processing and Control, 2023, 86(C), 105319. https://doi.org/10.1016/j.bspc.2023.105319

28. Yan, J., Chen, Y., Xiao, Z., Zhang, S., Jiang, M., Wang, T., Zhang, T., Lv, J., Becker, B., Zhang, R., Zhu, D., Han, J., Yao, D., Kendrick, K. M., Liu, T., Jiang, X. Modeling Spatio-Temporal Patterns of Holistic Functional Brain Networks via Multi-Head Guided Attention Graph Neural Networks (Multi-Head GAGNNs). Medical Image Analysis, 2022, 80, 102518. https://doi.org/10.1016/j.media.2022.102518

29. Zhang, C., Zhang, Z., Feng, Z., Yi, L. Z. Joint Sparse Model with Coupled Dictionary for Medical Image Fusion. Biomed. Signal Process. Control., 2023, 79(Part), 104030. https://doi.org/10.1016/j.bspc.2022.104030

30. Zhang, L., Ning, G., Zhou, L., Liao, H. E. Symmetric Pyramid Network for Medical Image Inverse Consistent Diffeomorphic Registration. Computerized Medical Imaging and Graphics, 2023, 104, 102184. https://doi.org/10.1016/j.compmedimag.2023.102184

31. Zhao, J., Li, Q., Li, X., Li, H. F., Zhang, L. Automated Segmentation of Cervical Nuclei in Pap Smear Images Using Deformable Multi-Path Ensemble Model. 2019 IEEE 16th International Symposium on Biomedical Imaging (ISBI 2019), IEEE, 2019, 1514-1515. https://doi.org/10.1109/ISBI.2019.8759262